Relationship between Bone Tissue Strain and Lattice Strain of HAp Crystals in Bovine Cortical Bone under Tensile Loading

Kazuhiro FUJISAKI[1] and Shigeru TADANO[2]

[1] Doctor Course Student, Division of Human Mechanical Systems and Design, Graduate School of Engineering, Hokkaido University, 060-8628, Japan

[2] Division of Human Mechanical Systems and Design, Graduate School of Engineering, Hokkaido University, 060-8628, Japan

Corresponding author:

Shigeru TADANO, PhD

Professor, Division of Human Mechanical Systems and Design, Graduate School of Engineering, Hokkaido University, N13 W8, Kita-ku, Sapporo, 060-8628, Japan

TEL & FAX: +81-11-706-6405, E-mail: tadano@eng.hokudai.ac.jp

Keywords:

Biomechanics, X-ray Diffraction, Cortical Bone, Hydroxyapatite, Strain Measurement

Manuscript type: Original Articles

Running title: Bone Tissue Strain and Lattice Strain of HAp, Fujisaki et al.

Word count: 3190 words (Introduction through Concluding Remarks)

ABSTRACT

Cortical Bone is a composite material composed of hydroxyapatite (HAp) and collagen. As HAp is a crystalline structure, an X-ray diffraction method is available to measure the strain of HAp crystals. However, HAp crystals in bone tissue have been known to have the low degree of crystallization. Authors have proposed an X-ray diffraction method to measure the lattice strain of HAp crystals from the diffusive intensity profile due to low crystallinity. The precision of strain measurement was greatly improved by this method. In order to confirm the possibility of estimating the bone tissue strain with measurements of the strain of HAp crystals, this work investigates the relationship between bone tissue strain on a macroscopic scale and the lattice strain of HAp crystals on a microscopic scale. The X-ray diffraction experiments were performed under tensile loading. Strip bone specimens of 40×6×0.8 mm in size were cut from the cortical region of a shaft of bovine femur. A stepwise tensile load was applied in the longitudinal direction of the specimen. By detecting the diffracted X-ray beam transmitted through the specimen, the lattice strain was directly measured in the loading direction. As a result, the lattice strain of HAp crystals showed lower value than the bone tissue strain measured by a strain gage. The bone tissue strain was described with the mean lattice strain of the HAp crystals and the elastic modulus.

Keywords:

Biomechanics, X-ray Diffraction, Cortical Bone, Hydroxyapatite, Strain Measurement

1. INTRODUCTION

On the microscopic scale, cortical bone is generally considered a composite of hydroxyapatite like mineral particles (HAp) and collagen matrix. Because the mineral particles are much stiffer than the collagen fiber matrix, bone stiffness is strongly influenced by the structure of the mineral HAp in bone tissue. The deformation behavior of HAp particles under external loading is important to understand the mechanical properties of bone, and as HAp in cortical bone has a crystalline structure, X-ray diffraction may be used to measure the lattice strain of HAp crystals.

A nondestructive and noninvasive method is necessary to investigate the stress or strain state of bone tissue in vivo. Cheng et al. (1995) have used elastic wave propagation to measure the nondestructive elastic modulus of the human tibia, and X-ray diffraction is used to measure the stress or strain in engineering and industrial application nondestructively. However, few researchers have applied X-ray diffraction to strain measurement of living bone tissue in vitro. Tadano and Todoh et al. (1999, 2000) confirmed that X-ray diffraction method was used to measure the stress in bone tissue and reported the residual stresses or strains in intact bone using polychromatic X-rays. However, HAp mineral particles have a much lower crystallinity than other crystalline materials (Raquel, 1981; Matsushima et al., 1986), and it is difficult to make a quantitative determination of the lattice strain in HAp from the peak positions of a diffusive diffraction profile.

An X-ray diffraction method to determine the lattice strain of crystals with low degrees of crystallization has been proposed (Fujisaki and Tadano et al., 2005). This method estimates the lattice strain of HAp from the whole of the diffraction profile of the X-ray intensity rather than only the peak position. To evaluate the stress of cortical bone, the bone tissue strain on the macroscopic scale must be estimated from measurement of the lattice strain on the

microscopic scale using X-ray diffraction, and this work investigated the relationship between the strain of cortical bone and the strain of HAp crystals under tensile loading. Two types of bone specimens (40×6×0.8 mm in size) were cut from the cortical region of the shaft of a bovine femur. They were longitudinally aligned with the bone axis or with the circumferential axis. The tensile load was applied stepwise during the X-ray irradiation, and the strain of the HAp crystals in the loading direction was directly measured by the X-ray beam diffracted and transmitted through the bone specimen.

2. STRAIN MEASUREMENTS OF HAP CRYSTALS

2.1 X-ray Diffraction Method with Transmitted Beam

Figure 1 shows an incident and transmitted beam path of a diffracted X-ray through a bone strip specimen. When X-rays are irradiated at HAp crystals in bone tissue, diffraction of the X-rays occurs in specific directions by scattering X-rays from each atom. The beam path of the diffracted X-rays is related to the interplanar spacing at a specific lattice plane (*hkl*) in HAp crystals. Using characteristic X-rays with a wavelength λ, a diffracted angle θ can be obtained by observing the peak position of the diffracted intensity of the X-rays. Bragg's law for X-ray diffraction phenomena is expressed as

$$2d \sin\theta = \lambda \tag{1}$$

where d is the width of the interplanar space between adjacent lattice planes of HAp crystals.

When deforming a specimen, the width of the interplanar spacing changes. The lattice strain ε_l at a specific lattice plane (*hkl*) is defined as the ratio between the width d^0 at the

non-strained state and the width d at the strained state. This relation is described by equation (2), where θ^0 and θ are the diffraction angles of the non-strained and strained states.

$$\varepsilon_l = \frac{d - d^0}{d^0} = \frac{\sin\theta^0 - \sin\theta}{\sin\theta} \tag{2}$$

When the direction of the external loading is aligned with the longitudinal axis of a specimen, as shown in Fig. 1, some X-rays diffracted from a specific lattice plane are transmitted through the specimen and emerge from the other surface. By detecting the X-ray beam, the lattice strain component in the same direction as the loading can be measured directly by this method.

2.2 Optimal Strain Search from the Intensity Profile of X-ray Diffraction

Figure 2 shows a schematic diagram of an intensity-angle profile of X-ray diffraction. In a highly crystallized material, a diffracted angle, 2θ, is obtained simply from the peak position of the high intensity profile according to the lattice spacing (*hkl*). The HAp structure in living bone has a low degree of crystallinity similar to metals. The HAp profile is diffused over a relatively wide 2θ range, and it is difficult to determine a peak position accurately.

The authors have proposed a method to estimate the lattice strain with high reliability even for low crystallinity compounds such as HAp particles in bone tissue (Fujisaki and Tadano et al., 2005). This method calculates the lattice strain using the whole diffraction profile rather than the peak position alone. Figure 3 shows the profiles of the diffracted intensity and the diffracted angle of strained and non-strained states. After the tensile deformation the profile moves to smaller angles because of the increase in interplanar spacing of lattice planes. The peak position and all of the non-strained state profiles are assumed to shift by the deformation.

The non-strained profile is divided into *n* regions. With the deformation of a specimen, every point ($2\theta^0_i$, I^0_i) on the non-strained profile shifts to a point ($2\theta^s_i$, I^s_i) on the strained profile. Each value of the angle can be calculated by equation (3) with the assumption of a constant strain, ε, defined as the point ($2\theta^c_i$, I^c_i) on the strained profile.

$$2\theta_i^c = 2\sin^{-1}\left\{\frac{\sin\left(2\theta_i^0/2\right)}{\varepsilon+1}\right\} \qquad (3)$$
$$I_i^c = I_i^0 \quad (i = 1,2,3,\cdots,\mathrm{n})$$

Equation (3) is derived from equations (1) and (2), and I is the diffracted intensity which is assumed not to change with the increase in the strain on the specimen. The strained values ($2\theta^c_i$, I^c_i) are equated with the points ($2\theta^s_i$, I^s_i) values on the experimentally obtained strained state profile. To determine the differences between the estimated and measured strain state profiles, an X-ray intensity at a diffracted angle position 2θ corresponding to a measurement step on the measured profile is determined with the estimated profile. The I^c_i value is determined by interpolating from the calculated intensity I^c_{i-1}, I^c_{i+1} as the direct proportional relationship. The difference between the estimated and measured strain state profile is expressed as equation (4),

$$F = \sum_{i=1}^{n} I_i^s \left(I_i^s - I_i^c\right)^2 \qquad (4)$$

which is weighted by the intensity value at each angle. The strain ε in equation (3) is set as a variable increasing step by step in the processing, and an optimal strain was established, where F attained the minimum value.

3. Experimental Procedure

3.1 Specimens

The specimens were made from the shaft of a bovine femur as indicated in Figure 4. The conditions of each specimen was unified according to the following procedure. A fresh bovine femur of a 5 year-old female was frozen at -35 °C prior to the experiments. After thawing out for 24 hours at room temperature (25 ± 3 °C and relative humidity of 55%), 40×6×0.8 mm strip shaped specimens were cut from the cortical bone in the shaft of the bovine femur. The longitudinal direction of a specimen was aligned with the bone axis (specimen A (n=12)) or with the circumferential axis (specimen B (n=6)). The surface of the specimens was polished with diamond powder. Each specimen was cleaned in an ultrasonic bath in physiological saline to eliminate undesired shavings and then dried out for 24 hours at room temperature. To measure the bone tissue strain on a macroscopic scale, a strain-gage was glued to the region not affected by the X-ray irradiation. The experiments were conducted at 25 °C and a relative humidity of 55% to maintain the specimens at a uniform doryness during the X-ray measurement.

3.2 X-ray Measurement System

Figure 5 shows an X-ray diffraction system (RINT2000, Rigaku Co., Japan) used here. Characteristic X-rays (Mo-Kα) were generated by a Mo target, and diffracted X-rays were measured as an intensity-angle profile by a scintillation counter moving on the path of the 2θ angle from 11° to 23°. Details of the X-ray conditions of the X-rays are listed in Table 1. In the X-ray irradiation, a tensile load was applied stepwise to the specimens using the device shown in Figure 6. The device generates the tensile load in the longitudinal direction of the specimen by the turning of a screw. A load cell was attached in the device to measure the tensile load. The specimens were deformed, stepwise at constant tensile strains of 500, 1000,

1500, and 2000 $\times 10^{-6}$ (micro strain) determined by a strain-gage. This strain is defined as the bone tissue strain ε_b, and during the tensile loading, three lattice strains, ε_l, at each of the lattice planes (002), (211) and (213) in the HAp crystals were measured by the X-ray diffraction system.

4. RESULTS

The elastic modulus of the specimens was obtained from the relationship between the tensile load and the bone tissue strain. The values of the elastic modulus were 27.9 ± 4.1 GPa (mean ± S.D.) for specimen A (n=12) and 19.6 ± 2.8 GPa for specimen B (n=6).

Figure 7 shows the X-ray diffraction profiles obtained from the bone specimens. The profiles were obtained by scanning 2θ from 11° to 23° with no deformation of the specimens. Three clear peaks appear in the profile at angles corresponding to the (002), (211) and (213) planes of the HAp crystals, classified as typical planes of a hexagonal (6/m) structure (Mason and Berry, 1968). The strain was calculated from the X-ray diffraction profiles at the non-strained and the strained state. There were only very small variations in the intensity values at the peak positions and shapes of the X-ray diffraction profiles at the non-strained and the strained states in this condition. Before the treatment for the strain calculations, the profile was smoothed by a simple moving average using 71 data points of all the 2401 data sets of 2θ from 11° to 23°. The background intensity was removed in the same manner as in the previous report (Fujisaki and Tadano et al., 2005). The lattice strains ε_l were calculated by the optimal values of equation (4) in the 11° to 12.5° range for the (002) plane, 13° to 16° for the (211) plane, and 21.5° to 23° for the (213) plane. The strain in equation (3) was set as a variable increasing 1 [micro-strain] in every calculation step.

Figures 8 and 9 show the relationship between the bone tissue strain ε_b and the lattice strain ε_l of specimens A and B. The lattice strain increased linearly with the bone tissue strain, all lattice strain was everywhere lower than the bone tissue strain. In specimen A, the strain ratio ($\varepsilon_l/\varepsilon_b$) was higher for the (002) plane than for the other two planes. The strain values of the (002) and (213) planes in specimen B could not be measured due to their low intensity as shown in Fig. 7. Although a constant macroscopic strain was applied to the specimens, the lattice strain showed different values for the different lattice planes, showing that it is not sufficient to determine the bone tissue strain simply from the lattice strain.

When the mean value $\overline{\varepsilon_l}$ of the lattice strain is defined as the optimal value calculated with equation (4) over the wide range of angles from 11° to 23°, Figure 10 shows the relationship between the bone tissue strain and the mean lattice strain $\overline{\varepsilon_l}$ in specimens A and B. The values of $\overline{\varepsilon_l}$ increase linearly with the bone tissue strain, and does not depend on the lattice plane of the HAp crystals. The mean strain ratio ($\overline{\varepsilon_l}/\varepsilon_b$) was higher for specimen A than for specimen B. This appears to agree with the differences in the elastic modulus of specimens A and B. The relationship between the strain ratio ($\varepsilon_l/\varepsilon_b$) and elastic modulus E_b [GPa] of all lattice planes are shown in Figure 11. Suggesting that, there is no apparent linear relation in the elastic modulus. Figure 12 shows the relationship between the mean strain ratio ($\overline{\varepsilon_l}/\varepsilon_b$) and the elastic modulus E_b [GPa], and here the bone specimens with higher elastic modulus have the higher values of mean strain ratios. The relationship appears linear and is approximated by

$$E_b = 36.8 \cdot \left(\overline{\varepsilon_l} / \varepsilon_b\right) + 5.3 \tag{5}$$

The bone tissue strain on the macroscopic scale can be obtained from the mean value of the lattice strains $\overline{\varepsilon_l}$ on the microscopic scale and the elastic modulus of the bone tissue E_b as

$$\varepsilon_b = \frac{36.8}{E_b - 5.3} \cdot \overline{\varepsilon_l} \tag{6}$$

5. DISCUSSION

This study investigated the relationship between bone tissue strain and lattice strain of HAp crystals with the lattice strain of the tensile loading direction measured directly by the X-ray beam diffracted and transmitted through the bone specimen. Because the X-ray intensity is an important factor for in the precision of strain measurements, specimens that are sufficiently thin have to be prepared for the X-ray diffraction experiments. The intensity of X-rays decreases exponentially with penetration depth, expressed by $I_{out} / I_{in} = e^{-mx}$, with incident X-ray intensity I_{in}, penetrating X-ray intensity I_{out}, X-ray absorption coefficient m, and penetration depth x. An X-ray absorption coefficient (mean ± S.D.) of 1.53 ± 0.07 [1/mm] was measured for all specimens. When the X-rays penetrate perpendicular to the surface of the specimens and is transmitted through the t = 0.8 mm thickness, the intensity was reduced by 30%. The path of the X-rays in this experiment is expressed by t / cos (θ). The reduction of intensity was very nearly 30%. The thickness of a specimen should be as small as possible to obtain a higher transmitted X-ray intensity. However, because the osteon size of cortical bone is about 0.1 ~ 0.2 mm, measurements of macroscopic bone tissue strains of specimens must consider this.

The crystal orientation of HAp crystals in bovine femurs is known to be that the (002) plane, aligned with the bone axis (Sasaki and Sudoh, 1997). In this work, the lattice strain of the (002) plane was larger than the lattice strains of the other planes under constant tensile deformation. The mean value of the lattice strains $\overline{\varepsilon_l}$ was defined as an average of each lattice strain weighted by the intensity of the diffracted X-rays. The main lattice plane was oriented at the (002) and (211) planes for specimen A, and for the (211) plane only for specimen B, and the elastic modulus of cortical bone may be determined by differences between these. Sasaki et al. (1989) have estimated an anisotropic elastic modulus from the degree of crystal orientation of the (002) plane in bovine femurs. This result used the lattice strain to show the need for further study of the relationship between the crystal orientation and the anisotropic elastic modulus of cortical bone.

The cortical region of a long bone is known to have an anisotropic structure (Wainwright et al., 1976). The human femur consisting of Haversian bone has been considered to be transversely isotropic (Van Buskirk et al., 1981). Pithioux et al. (2002) have measured, nondestructively, the anisotropic elastic modulus of bovine cortical bone on the assumption of an orthotropic lamellar structure using ultrasonic wave propagation. There is a significant difference in the elastic moduli in the axial and circumferential directions in cortical bone. Rho et al. (2002) performed nano-indentation tests at the osteon level to estimate the elastic modulus of bone tissue, and described an anisotropy produced on the Haversian system. However, the anisotropic elastic modulus should be explained from the microstructure of the HAp crystals and collagen matrix. The lattice strain measured in this experiment showed lower values than the macroscopic strain, and was very different in each specimen even when applying a constant macroscopic strain. The work reported here attempted to establish the relationship between the elastic modulus of specimens and the lattice strain of HAp crystals, and two types of specimen with clearly different elastic moduli

from the shaft of a bovine femur were used. The lattice strain showed higher values for bone axial specimens (A) than for outside circumferential specimens (B). In general, the elastic modulus of bone is considered to originate in the force bearing serial portions of HAp mineral particles. Such a mechanical structure can be attributed to the preferred orientation of bone mineral. These results indicate that the lattice strain of HAp is influenced by the elastic modulus of the specimen.

Here, the resolution of the strain measurements was determined based on the strain step set in the calculations of the strained state profile. The measured strains had a data spread with a standard deviation of ±100 [micro-strain] at all strain values. The accuracy of the X-ray strain measurements depend on the intensity of the incident X-rays and the resolution of the scanning steps. Using strong X-rays or highly sensitive X-ray detection devices and a high resolution scanning system, the lattice strain could be measured with high precision.

The relative humidity of 55% here was needed for gluing the strain gage to the specimen surface, and is different from the physiological state. The mechanical properties of such bone are different from that measured in physiological saline (Sasaki et al., 1995). It is known that the elastic modulus of bone in wet conditions becomes lower than in dry conditions. The elastic modulus of collagen decreases with increased moisture. In equation (6), the lattice strain of HAp under constant bone tissue strain depends on the elastic modulus of the specimen, and with equation (6), the strain of HAp would decrease in the living body.

The X-ray irradiated region was about 2 mm for square on the surface of the specimens and the lattice strain was measured as an average value for this area. Nicolella et al. (2001) developed a strain distribution measurement for the surface of cortical bone at the microscopic level using micro-structural imaging, and investigated the strain concentration around a micro crack. The stress concentration is important for understanding of bone

fractures, and by adding a micro focus X-ray beam to this strain measurement system, the lattice strain at an inner area of the specimen can be obtained and used in micro crack studies.

Much is still unknown about the structure of HAp crystals and collagen fibres and the shape of HAp particles (Sasaki et al., 2002). A determination of the strain of HAp crystals in bone tissue under loading is important for an understanding of the composite characteristics of HAp crystals and collagen fibres in bone. The method to calculate the lattice strain not using a peak position but from the whole of the diffraction profile used here resulted in improved accuracy of the strain measurements in the bone tissue. This report shows the relationship between the macroscopic and microscopic strains of HAp with crystal orientation and elastic modulus. Details of this relationship can be in evaluating the microscopic structure and characteristics of bone.

7. CONCLUDING REMARKS

The lattice strain of HAp crystals aligned with a loading direction was obtained directly from diffracted and transmitted X-ray beams measured after penetration of cortical bone specimens under tensile loading. The lattice strain was lower than the macroscopic bone tissue strain in all specimens and higher for specimens with higher elastic modulus under similar macroscopic strains. The bone tissue strain could be estimated from the lattice strain calculated for the whole profile and the elastic modulus of the bone tissue.

ACKNOWLEDGEMENTS

This work was supported by Grant-in-Aid for Scientific Research (B) (2), MEXT (No.16300143).

REFERENCES

Cheng, S., Timonen, J., Suominen, H., 1995. Elastic wave propagation in bone in vivo: Methodology, J. Biomechanics 28(4), 471-478.

Fujisaki, K., Tadano, S., Sasaki, N., 2005. A method on strain measurement of HAP in cortical bone from diffusive profile of X-ray diffraction, J. Biomechanics (in press).

Mason, B., Berry, L. G., Elements of mineralogy, 1968, Freeman and Company, U. S. A., 387.

Matsushima, N., Tokita, M., Hikichi, K., 1986. X-ray determination of the crystallinity in bone tissue, Biomechanica et Biophysica Acta 883, 574-579.

Nicolella, D. P., Nicholls, A. E., Lankford, J., Davy, D. T., 2001, Machine vision photogrammetry: a technique for measurement of microstructural strain in cortical bone, J. Biomechanics 34, 135-139.

Pithioux, M., Lasaygues, P., Chabrand, P., 2002. An alternative ultrasonic method for measuring the elastic properties of cortical bone, J. Biomechanics 35, 961-968.

Raquel, Z. L., 1981. Apatites in biological systems, Prg. Crystal Growth and Characterization of Materials 4, 1-45.

Rho, J. Y., Zioupos, P., Currey, J. D. and Pharr, G. M., 2002. Microstructural elasticity and regional heterogeneity in human femoral bone of various ages examined by nano-indentation, J. Biomechanics 35, 189-198.

Sasaki, N., Enyo, A., 1995. Viscoelastic properties of bone as a function of water content, J. Biomechanics 28, 809-815.

Sasaki, N., Matushima, N., Ikawa, T., Yamamura, H., Fukuda, A., 1989, Orientation of bone mineral and its role in the anisotropic mechanical properties of bone – transverse anisotropy, J. Biomechanics 22, 157-164.

Sasaki, N., Sudoh, Y., 1997. X-ray pole figure analysis of apatite crystals and collagen molecules in bone, Calcif Tissue Int. 60, 361-367.

Sasaki, N., Tagami, A., Goto, T., Taniguchi, M., Nakata, M. and Hikichi, K., 2002. Atomic force microscopic studies on the structure of bovine femoral cortical bone at the collagen fibril-mineral level, J. Materials Science: Materials in Medicine 13, 333-337.

Tadano, S., Okoshi, T. and Shibano, J., 2000. Residual stress induced from bone structure and tissue in rabbit's tibia, Proc. of 10th Int. Conf. on Biomedical Eng., 529-530.

Tadano S. and Todoh M., 1999. Anisotropic residual stress measurements in compact bone using polychromatic X-ray diffraction, In: Pedersen, P. and Bendisøe, M. (Ed.), IUTAM Symposium on Synthesis in Bio Solid Mechanics, Klumer Academic Publications, Pordr Netherland, 139-159.

Todoh, M., Tadano S., Shibano J. and Ukai T., 2000. Polychromatic X-ray measurements of anisotropic residual stress in bovine femoral bone, JSME International Journal, Series C. 43-4, 795-801.

Van Buskirk, W. C. and Ashman, R. B., 1981. The elastic moduli of bone, In: Cowin, S. C. (Ed), Mechanical properties of bone, ASME, U. S. A., 131-143.

Wainwright, S. A., Biggs, W. D., Currey, J. D. and Gosline, J. M., 1976. Structure of bone; Mechanical properties of bone, In: Mechanical design in organisms, Edward Arnold Ltd., U. K.,160-187.

Figure and Table Legends

Fig. 1 The incident and transmitted beam paths of diffracted X-rays through a strip shaped bone specimen. X-rays diffracted from a specific lattice plane are transmitted though the specimen.

Fig. 2 The X-ray diffraction profiles measured from high crystallized material and low crystallized material. The HAp profile in cortical bone is diffusive due to low crystallinity.

Fig. 3 The profile of the diffracted intensities and diffracted angles in the strained and non-strained state.

Fig. 4 The bone specimen (40×6×0.8 mm in size) was cut from the cortical region of the shaft of a bovine femur. To measure the bone tissue strain on a macroscopic scale, a strain-gage was glued to the region not affected by the X-ray irradiation.

Fig. 5 X-ray measurement system (RINT2000, Rigaku Co.).

Fig. 6 The tensile loading device with specimen. The macroscopic bone tissue strain is measured by the strain-gage on the specimen surface and the tensile load is obtained from a load cell attached to the device.

Fig. 7 X-ray diffraction profiles of bone specimens A and B. There are representative peaks on the profiles for each lattice plane (*hkl*).

Fig. 8 Relationship between bone tissue strain ε_b and lattice strains ε_l (mean ± S.D. n=12) at the (002), (211) and (213) planes in specimen A.

Fig.9 Relationship between bone tissue strain ε_b and lattice strain ε_l (mean ± S.D. n=6) at the (211) plane in specimen B.

Fig. 10 Relationship between bone tissue strain ε_b and mean lattice strain $\overline{\varepsilon_l}$ in specimens A and B.

Fig. 11 Relationship between the elastic modulus of bone tissue E_b and the lattice strain to bone tissue strain ($\varepsilon_l / \varepsilon_b$) ratios in specimen A.

Fig. 12 Relationship between the elastic modulus of bone tissue E_b and the mean lattice strain to bone tissue strain ($\overline{\varepsilon_l} / \varepsilon_b$) ratios in specimens A and B.

Table 1 The X-rays generated from the Mo target in the RINT2000 system and the diffracted X-rays were measured by a scintillation counter under conditions listed here.

Figure 1

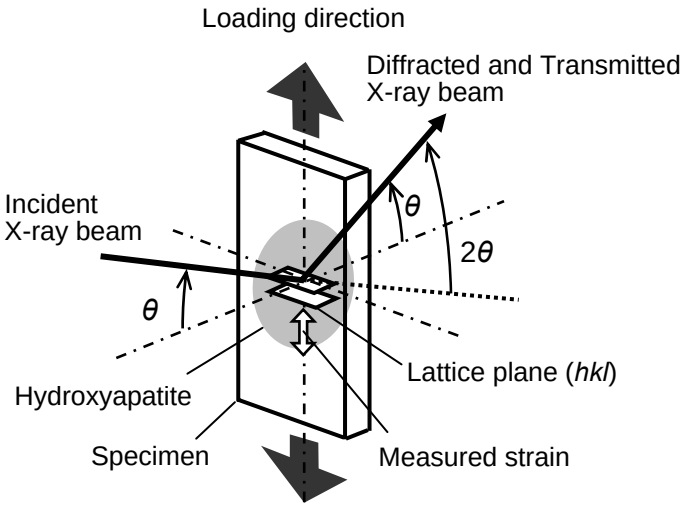
Loading direction
Diffracted and Transmitted
X-ray beam
Incident
X-ray beam
θ
2θ
θ
Lattice plane (hkl)
Hydroxyapatite
Specimen
Measured strain

Figure 2

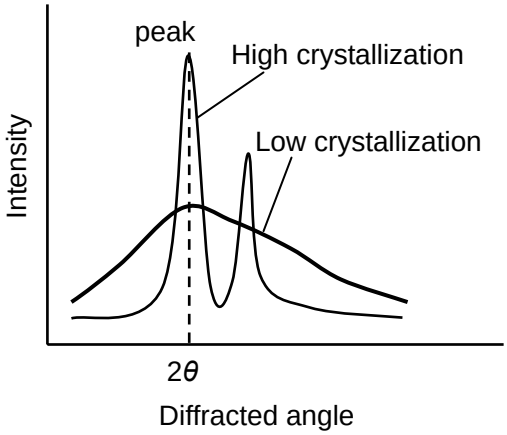
peak
High crystallization
Low crystallization
Intensity
2θ
Diffracted angle

Figure 3

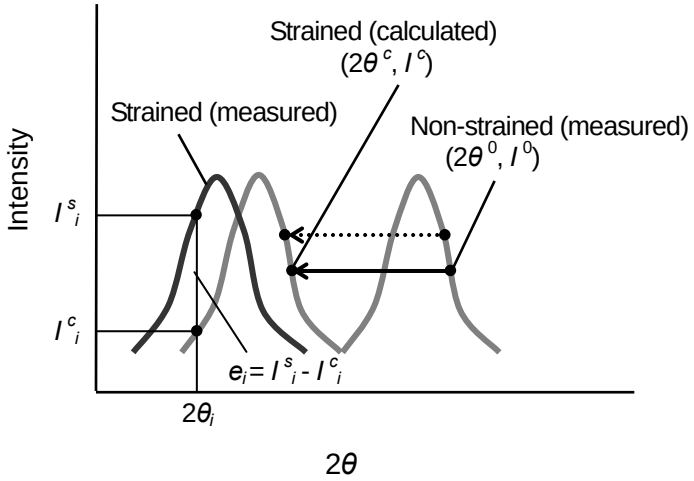
Strained (calculated)
(2θ c, I c)
Strained (measured)
Non-strained (measured)
(2θ 0, I 0)
Intensity
I s i
I c i
ei = I s i - I c i
2θi
2θ

Figure 4

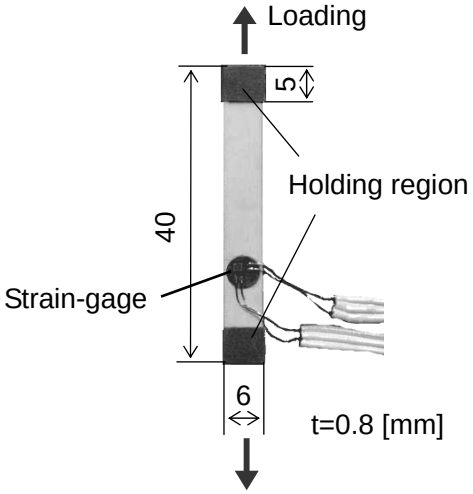

Figure 5

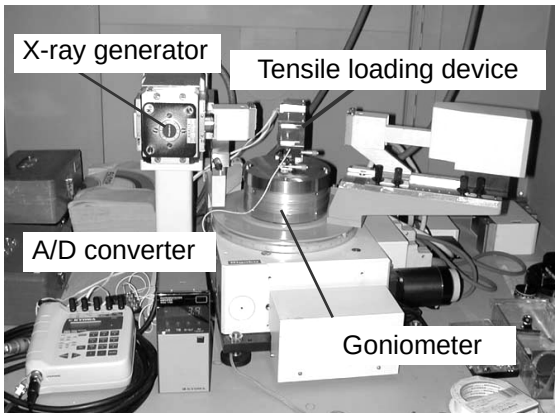
X-ray generator
Tensile loading device
A/D converter
Goniometer

Figure 6

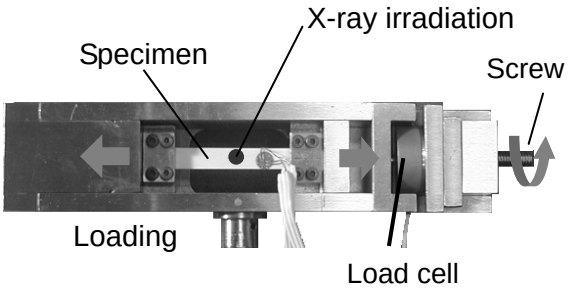

Figure 7

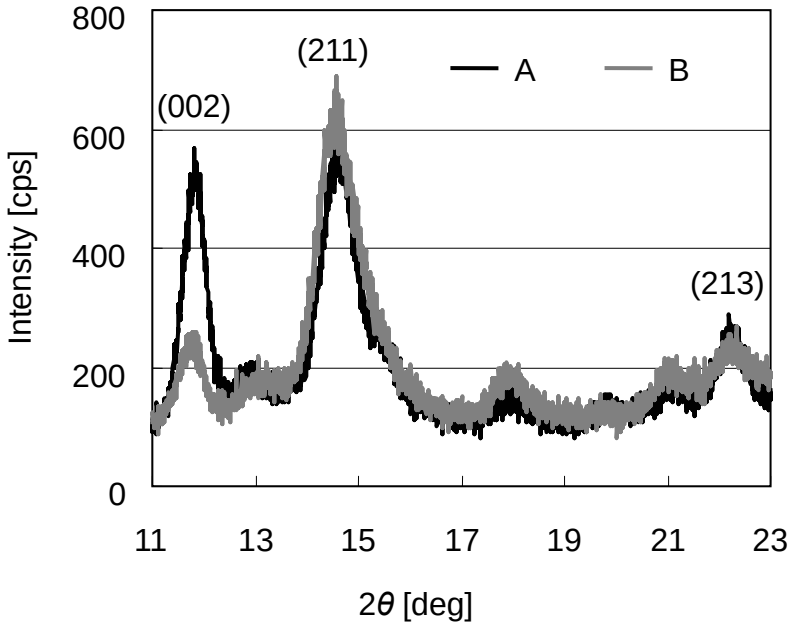
800
600
400
200
0
Intensity [cps]
(002)
(211)
(213)
A
B
11
13
15
17
19
21
23
2θ [deg]

Figure 8

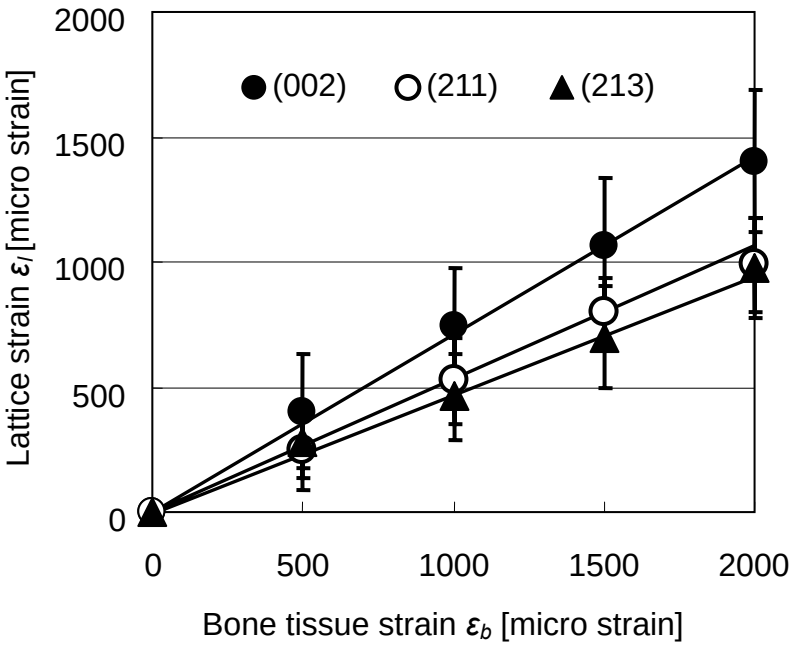
2000
1500
1000
500
0
(002)
(211)
(213)
Lattice strain ε_l [micro strain]
0
500
1000
1500
2000
Bone tissue strain ε_b [micro strain]

Figure 9

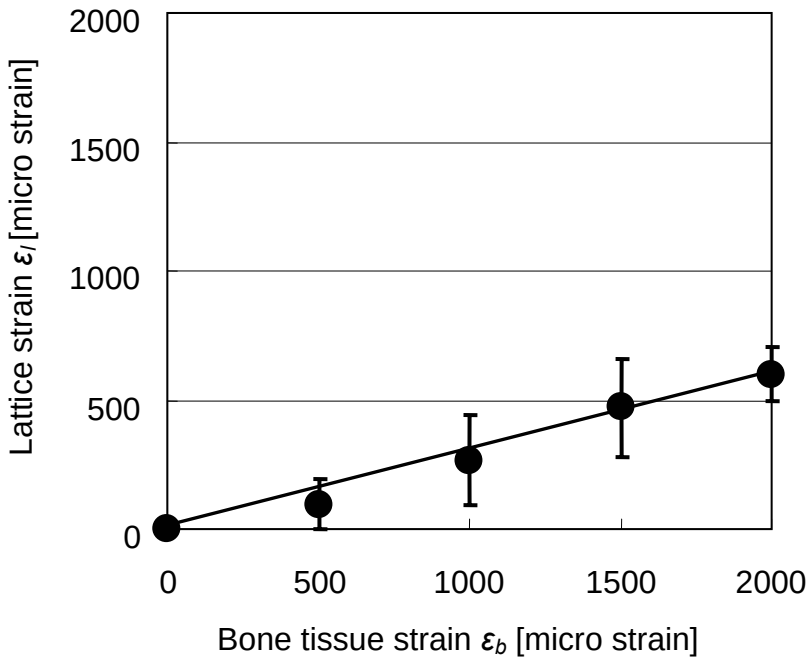
2000
1500
1000
500
0
Lattice strain ε_l [micro strain]
0
500
1000
1500
2000
Bone tissue strain ε_b [micro strain]

Figure 10

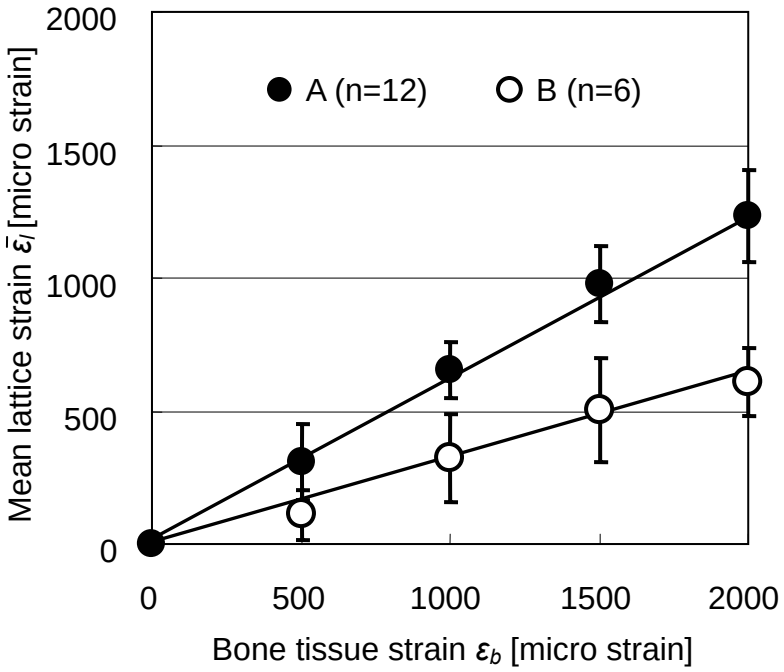
2000
1500
1000
500
0
Mean lattice strain $\bar{\varepsilon}_l$ [micro strain]
A (n=12)
B (n=6)
0
500
1000
1500
2000
Bone tissue strain ε_b [micro strain]

Figure 11

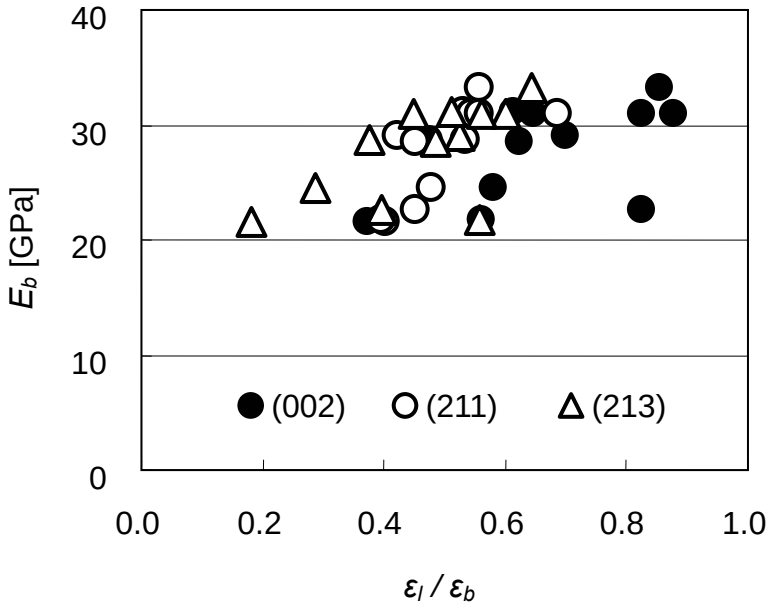
40
30
20
10
0
E_b [GPa]
0.0
0.2
0.4
0.6
0.8
1.0
$\varepsilon_l / \varepsilon_b$
(002)
(211)
(213)

Figure 12

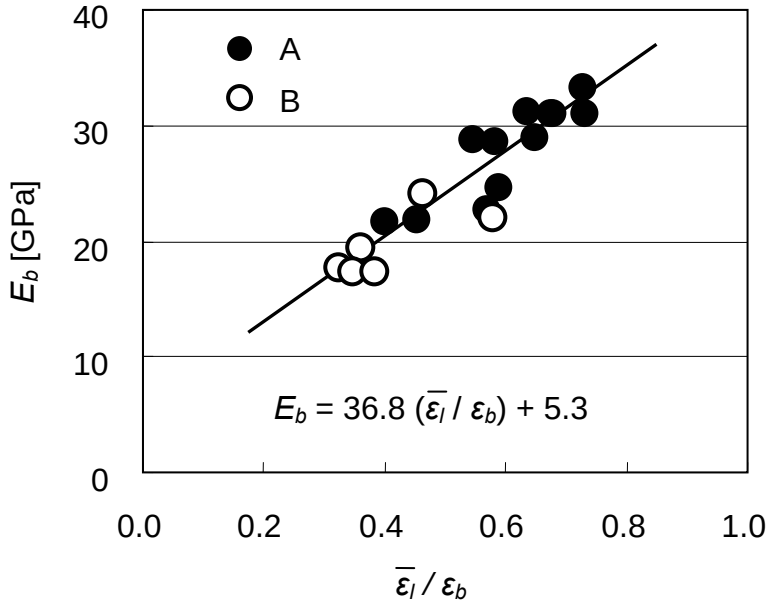
40
30
20
10
0
A
B
E_b [GPa]
E_b = 36.8 ($\bar{\varepsilon}_l$ / ε_b) + 5.3
0.0
0.2
0.4
0.6
0.8
1.0
$\bar{\varepsilon}_l$ / ε_b

Table 1

Target		Mo
Characteristic X-rays		Mo-Kα
Wave length λ	(nm)	0.07107
Filter		Zr
Tube voltage	(kV)	40
Tube current	(mA)	40
Measurement angle 2θ	(deg)	11~23
Scan speed	(deg/min)	2.0
Sampling width	(deg)	0.005